Int. J. Electrochem. Sci., 8 **(2013)** 703 - 719

International Journal of
ELECTROCHEMICAL
SCIENCE
www.electrochemsci.org

Electrochemical Properties of Nanosized Li_2MnO_3-$Li(Ni_{1/3}Co_{1/3}Mn_{1/3})O_2$ Composite Cathode Powders Prepared by Spray Pyrolysis

Mun Yeong Son[1], *Seung Ho Choi*[1], *Jung Yeul Yun*[2], *Hye Moon Lee*[2], *Yun Chan Kang*[1,*]

[1]Department of Chemical Engineering, Konkuk University, 1 Hwayang-dong, Gwangjin-gu, Seoul 143-701, Korea
[2]Functional Materials Division, Korea Institute of Materials Science, 531 Changwonadaero, Changwon, Gyeongnam 641-831, Korea
*E-mail: yckang@konkuk.ac.kr

Received: 28 October 2012 / *Accepted:* 22 November 2012 / *Published:* 1 January 2013

Nanosized $0.6Li_2MnO_3$–$0.4Li(Ni_{1/3}Mn_{1/3}Co_{1/3})O_2$ composite powders are prepared by spray pyrolysis at high post-treatment temperatures. The optimum concentrations of citric acid and ethylene glycol, selected as the appropriate organic additives to obtain the composite nanopowders, are 0.2 M each. The spherical precursor powders of large size, with hollow and porous structures, are converted into composite nanopowders. Transmission electron microscopy, X-ray diffraction, X-ray photoelectron spectroscopy, and the cycling properties of the powders indicate that the optimum post-treatment temperature for obtaining composite cathode nanopowders is 900 °C. The mean size of the composite powders post-treated at 900 °C is 136 nm. The composite cathode powders post-treated at 900 °C have high initial charge/discharge capacities of 350 and 291 mAh g^{-1}. The discharge capacity of the composite cathode powder post-treated at 900 °C decreases from 291 to 269 mAh g^{-1} by the 30th cycle, in which the capacity retention is 92.4%.

Keywords: cathode material; spray pyrolysis; composite material; nanomaterials

1. INTRODUCTION

To improve the electrochemical properties and performances of Li-ion batteries, many researchers have investigated Li-rich compounds [1-9]. Because of the characteristics of Li_2MnO_3, Li-rich cathode materials have high capacities and enhance cathode material properties [1-3]. So, Li-rich layered materials, $Li[Li_xM_{1-x}]O_2$ (M= Mn, Ni, Co, or combinations), have been studied as promising cathode materials for Li-ion batteries [4-6]. Many researchers have largely focused on Li-rich Ni–Co–Mn cathode materials such as xLi_2MnO_3–$(1-x)Li(Ni_{1/3}Mn_{1/3}Co_{1/3})O_2$ [7-9].

Li-rich cathode materials have the drawback of low rate capabilities [10-15]. Small particles of submicron size improve the rate capabilities of Li-rich cathode materials [16-21]. Many preparation methods, such as co-precipitation and sol–gel methods have been used in the preparation of fine-sized Li-rich cathode materials [22,23]. Nanosized cathode powders have high power densities because they can quickly diffuse Li^+ ions in materials at high current densities [24-26]. However, the preparation and characteristics of Li-rich cathode nanopowders have not been well studied.

Spray pyrolysis is a gas-phase reaction method. It is a useful way of preparing complex-component cathode powders with non-aggregated morphologies [27-34]. Recently, spray pyrolysis has been developed as a simple and scalable process for large-scale production of nanosized cathode powders [35,36]. Precursor powders of large size, with hollow and thin-walled structures, have been prepared under easily scalable preparation conditions, such as high flow rate of carrier gas, short residence time, and low preparation temperature. The precursor powders were converted into nanosized cathode powders after post-treatment at high temperatures and a simple milling process. The hollow morphology of the precursor powders decreased aggregation of the cathode powders at high post-treatment temperatures. In the preparation of submicron or micron-sized cathode powders by spray pyrolysis, the powders have to be prepared under restricted preparation conditions, which reduce the production rate of the cathode powders.

In this study, nanosized $0.6Li_2MnO_3$–$0.4Li(Ni_{1/3}Mn_{1/3}Co_{1/3})O_2$ composite cathode powders were prepared using a scalable spray pyrolysis process. The electrochemical and physical properties of the nanosized composite powders post-treated at temperatures between 600 and 1000 °C were investigated.

2. EXPERIMENTAL

Nanosized $0.6Li_2MnO_3$–$0.4Li(Ni_{1/3}Mn_{1/3}Co_{1/3})O_2$ composite powders were prepared using ultrasonic spray pyrolysis. A 1.7-MHz ultrasonic spray generator with six vibrators was used to generate a large amount of droplets. The inner diameter and the length of the quartz reactor were 55 mm and 1.2 m, respectively. The reactor temperature was maintained at 900 °C. The flow rate of the air used as the carrier gas was fixed at 20 L min^{-1}. The precursor powders prepared using spray pyrolysis were post-treated at various temperatures for 5 h in air. The precursor solutions were prepared by dissolving $LiNO_3$ (Junsei, 98%), $Ni(NO_3)_2{\cdot}6H_2O$ (Junsei, 98%), $Mn(NO_3)_2{\cdot}6H_2O$ (Junsei, 97%), and $Co(NO_3)_2{\cdot}6H_2O$ (Junsei, 98%) in distilled water. The Li component added to the spray solution was in excess of 3 wt%, which is the stoichiometric amount for forming the composite powders. The concentration of the spray solution was 0.5 M. Citric acid and ethylene glycol (EG) were used as chelating agents to facilitate the formation of hollow particles. The chelating agents also acted as the carbon source. The concentrations of citric acid and EG were each 0.2 M.

The crystal structures of the prepared cathode powders were investigated using X-ray diffractometry (XRD, X'pert PRO MPD) with Cu Kα radiation (λ = 1.5418 Å) at the Korea Basic Science Institute (Daegu). The morphological characteristics were investigated using scanning electron microscopy (SEM, JEOL JSM-6060) and high-resolution transmission electron microscopy (TEM, JEOL JEOL-2100F) at 200 kV. The powders were also examined using X-ray photoelectron spectroscopy (XPS, ESCALAB-210) with Al Kα radiation (1486.6 eV). The binding energy was calibrated with reference to the C 1s level of carbon (284.5 eV). The elemental compositions of the powders were investigated using an inductively coupled plasma-optical emission spectrometer (ICP-OES, Thermo elemental, ICAP 6000).

The charge/discharge capacities of the nanosized $0.6Li_2MnO_3$–$0.4Li(Ni_{1/3}Mn_{1/3}Co_{1/3})O_2$ composite powders were also measured. Each cathode electrode was made of 80 wt% active material, 10 wt% carbon black (Super-P) as a conductive material, and 10 wt% polytetrafluoroethylene (PTFE) binder with a few drops of alcohol. All the cathode electrodes were dried at 120 °C for 24 h under vacuum. Li metal and a microporous polypropylene film were used as the anode electrode and the separator, respectively. The electrolyte solution was 1 M $LiPF_6$ in a 1:1 mixture by volume of EC/DMC. The cells were assembled in a glove-box filled with pure argon. The charge/discharge characteristics of the samples were measured through cycling in the 2.0–4.8 V potential range at a constant current density of 20 mA g^{-1} with a coin cell (2032 type).

3. RESULTS AND DISCUSSION

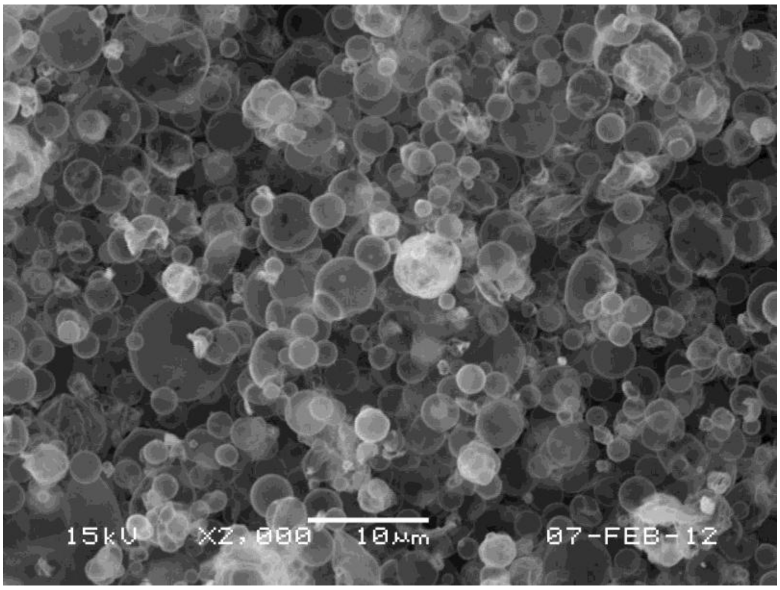

Figure 1. SEM image of the precursor powder prepared by spray pyrolysis.

The morphologies of the powders prepared by spray pyrolysis were affected by the preparation conditions and the properties of the spray solution. In this study, various types of organic additives were used to prepare precursor powders of large size, with hollow and thin-walled structures. The optimum concentrations of citric acid and EG, selected as appropriate organic additives, were each 0.2 M. The preparation conditions, such as flow rate of the carrier gas, preparation temperature, and solution concentration, were also optimized for preparing the precursor powders. The morphology of the precursor powder prepared under the optimum preparation conditions is shown in Fig. 1. The precursor powders were spherical, with hollow and porous structures. The mean size of the precursor powders, measured from the SEM images, was 2.2 μm. One precursor particle was formed from one droplet several microns in size. A number of precursor powders had larger sizes than those of the droplets generated by the transducer. Expansion of the precursor powders therefore occurred during drying and droplet decomposition. The drying and decomposition characteristics of the metal chelates, as well as the evolving gas formed by decomposition of organic additives and evaporation of water droplets, resulted in precursor powders with hollow structures.

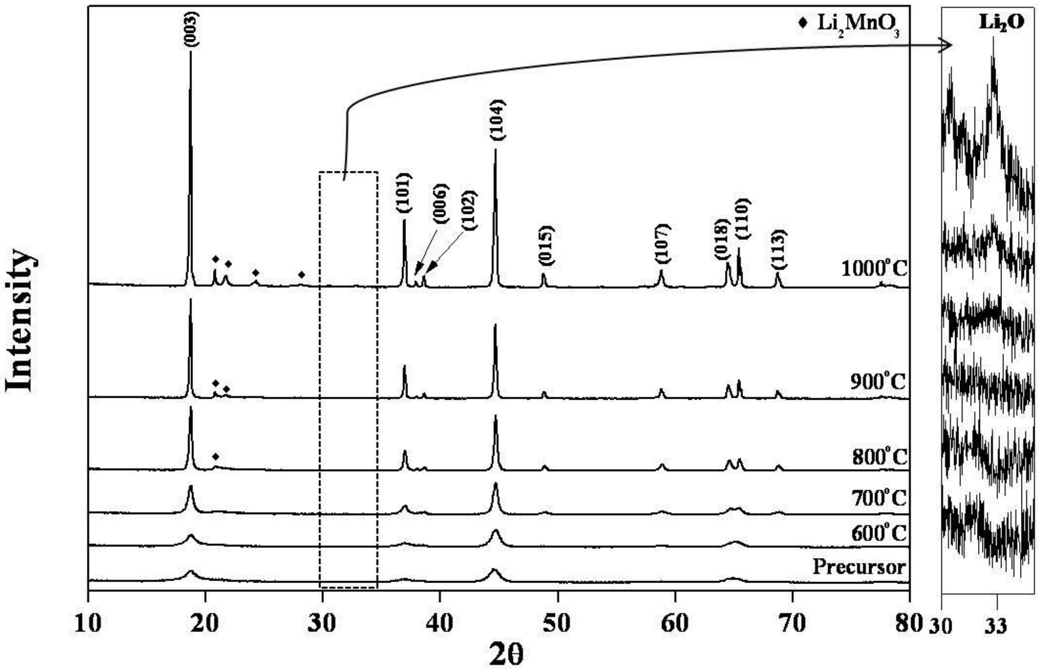

Figure 2. XRD patterns of the precursor and post-treated powders at various temperatures.

The precursor powders were post-treated at temperatures between 600 and 1000 °C to obtain the composite cathode powders. Fig. 2 shows the XRD patterns of the precursor and powders post-treated at various temperatures. The XRD peaks of the precursor powders prepared at 900 °C were broad with low peak intensities because of the short residence time of the powders inside the hot-wall reactor. The sharpness and intensities of the XRD peaks increased with increasing post-treatment temperature. The XRD peak near 21°, which can be attributed to the superlattice structure of Li_2MnO_3, appears above 800 °C [37-39]. The post-treated powders had a mixed-layered crystal structure of Li_2MnO_3 and $Li(Ni_{1/3}Mn_{1/3}Co_{1/3})O_2$ phases, and formed a composite compound. The XRD patterns of the powders post-treated at low temperatures, below 700 °C, had low intensity ratios of the (003) and (104) peaks. The ratio $I_{(003)}/I_{(104)}$ increases with increasing post-treatment temperature. The intensity ratios of the (003) and (104) peaks of the nanosized cathode powders post-treated at various temperatures are listed in Table 1.

Table 1. $I_{(003)}/I_{(104)}$ intensity ratio and mean crystallite sizes of the nanosized composite powders post-treated at various temperatures.

Post-treated temperatures	$I_{(003)}/I_{(104)}$	d(nm)
Precursor	-	7
600°C	0.78	8
700°C	0.9	14
800°C	1.2	22
900°C	1.3	29
1000°C	1.7	32

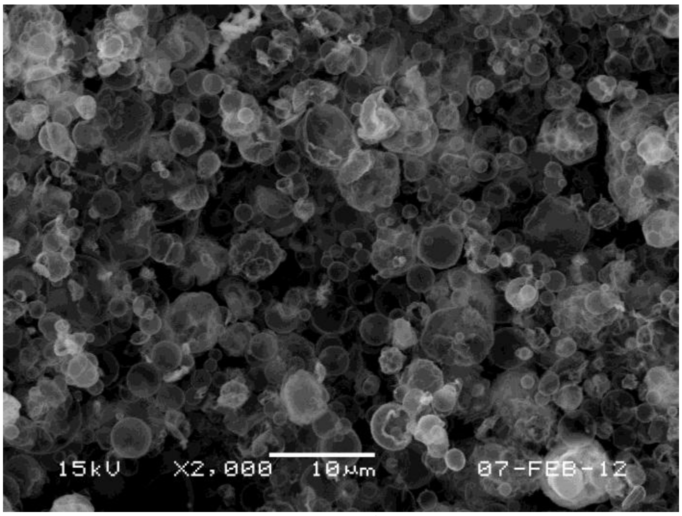

(a) 600°C

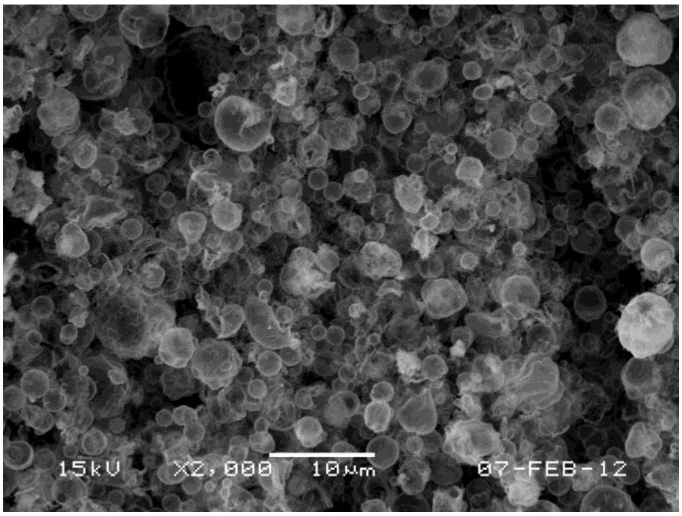

(b) 700°C

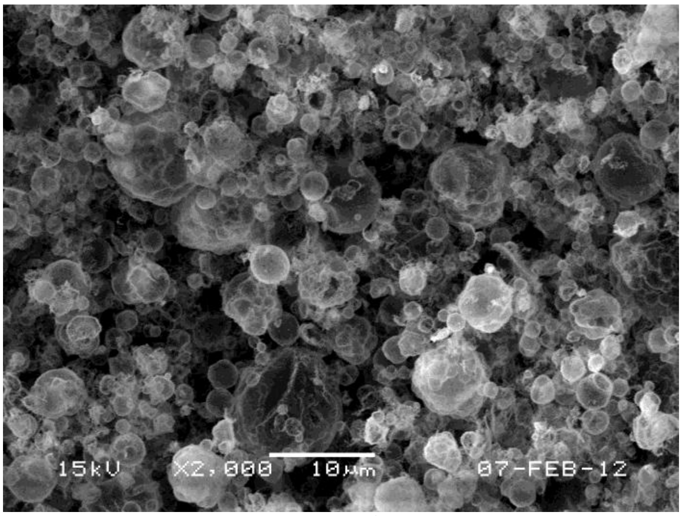

(c) 800°C

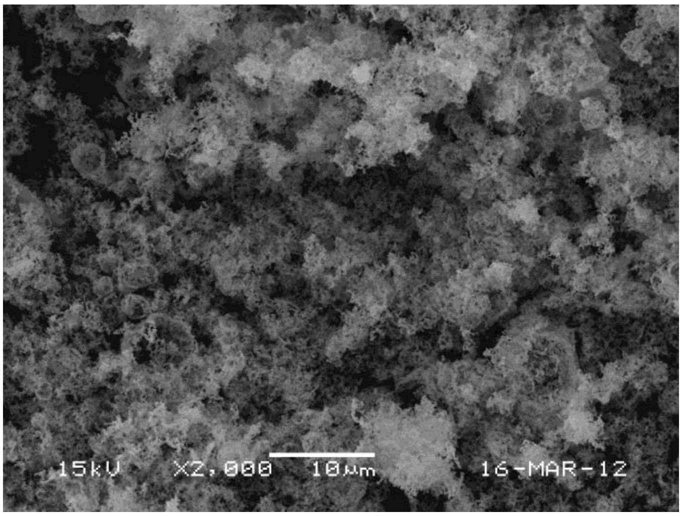

(d) 900°C

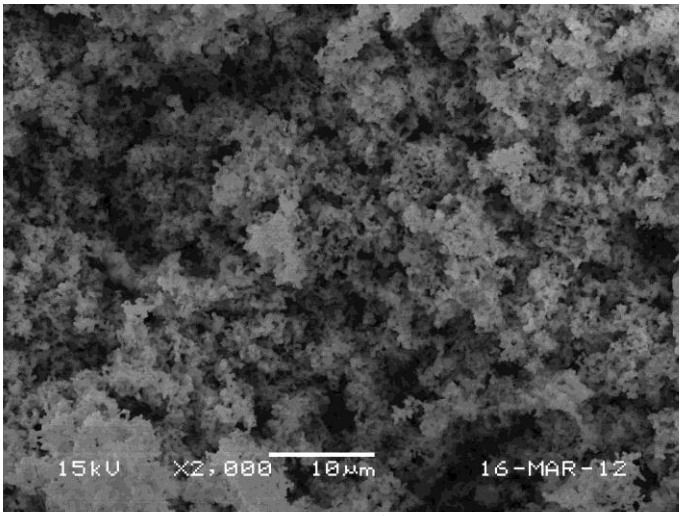

(e) 1000°C

Figure 3. SEM images of the composite powders post-treated at various temperatures before milling process.

As shown in Table 1, the $I_{(003)}/I_{(104)}$ ratios of the powders post-treated at 900 and 1000 °C were 1.34 and 1.71, respectively. This indicates that when the post-treatment temperatures are high, there is a low amount of cation mixing in the structures of the cathode powders prepared by spray pyrolysis [40]. The mean crystallite sizes of the composite powders measured by Scherrer's equation from the (003) peak widths of the XRD patterns are shown in Table 1. The composite powders had fine crystallite sizes even at a high post-treatment temperature of 1000 °C. Wang et al. reported that the peak near 33° in the XRD pattern of the composite powders is caused by the formation of an Li_2O phase by phase separation [41]. Phase separation of the composite powders post-treated at a high temperature of 1000 °C was also clearly seen in the XRD pattern, as shown by extended XRD patterns.

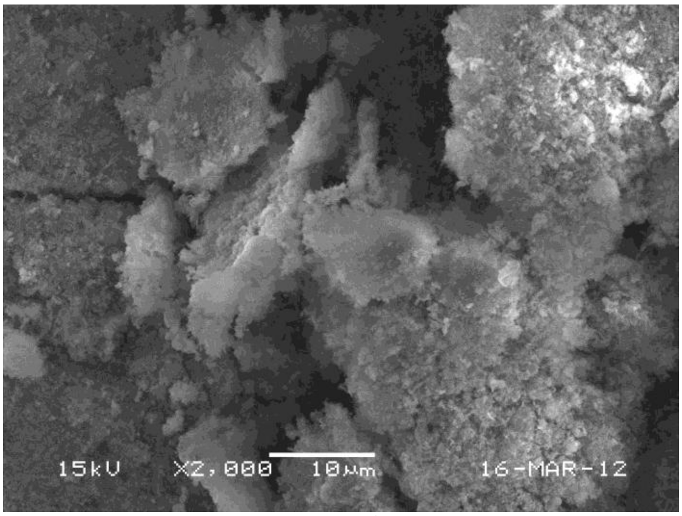

(a) 600°C

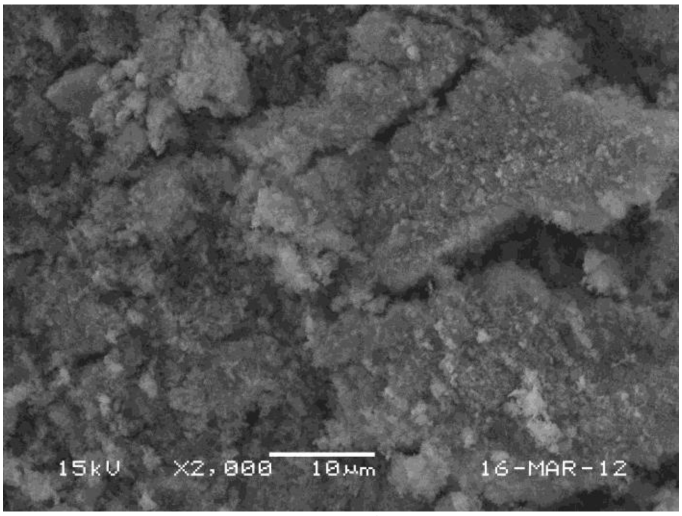

(b) 700°C

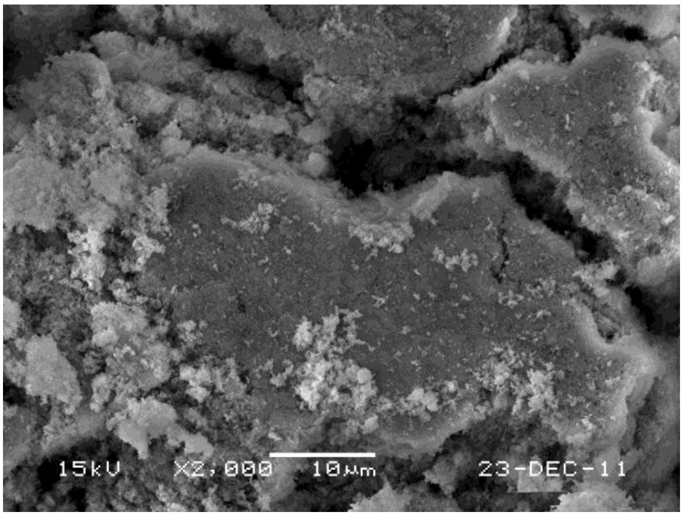

(c) 800^{o}C

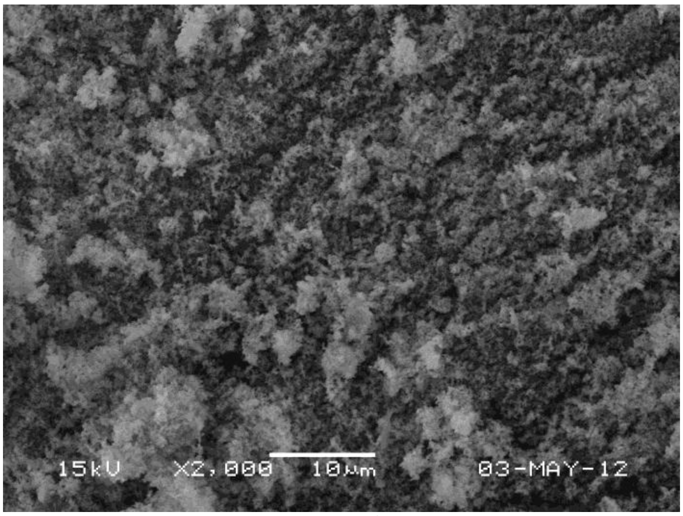

(d) 900^{o}C

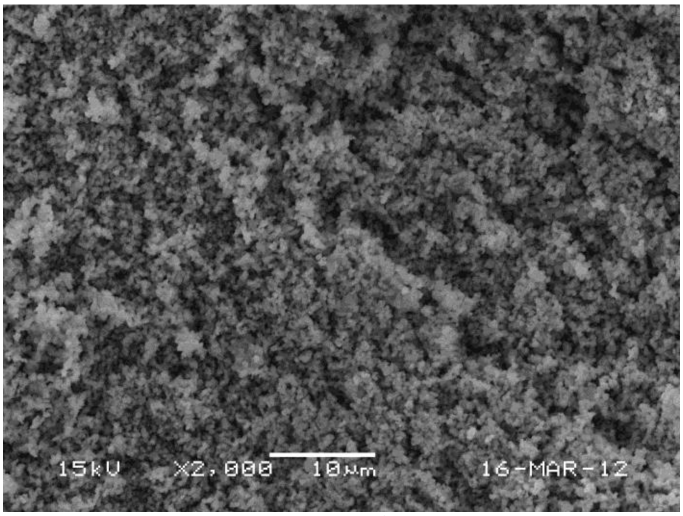

(e) 1000^{o}C

Figure 4. SEM images of the composite powders post-treated at various temperatures after simple milling process.

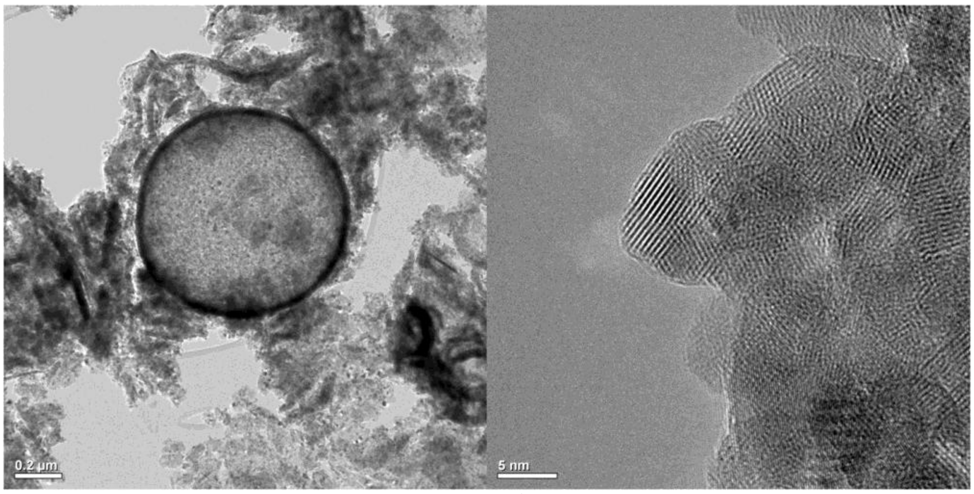

(a) 600°C

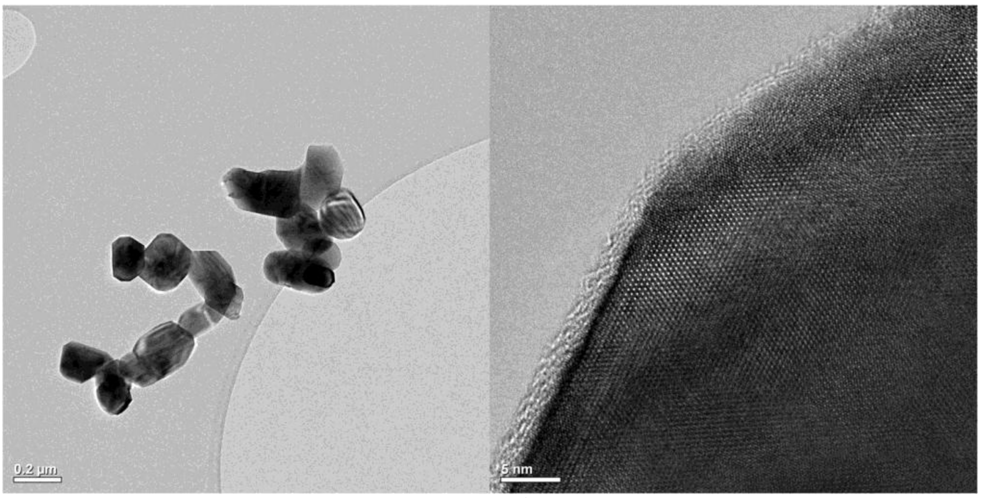

(b) 900°C

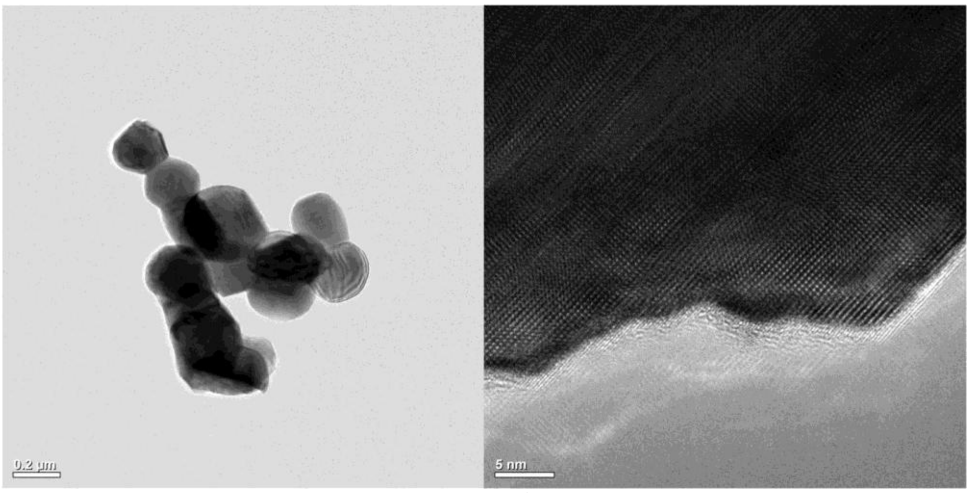

(c) 1000°C

Figure 5. TEM images of the nanosized composite powders post-treated at various temperatures.

The morphologies of the Li-rich cathode powders post-treated at various temperatures before milling are shown in Fig. 3. The cathode powders post-treated at temperatures below 800 °C maintained the spherical shapes with thin-walled structures of the precursor powders. The cathode powders post-treated at high temperatures of 900 and 1000 °C had fine grain sizes and loosely aggregated structures. The post-treated composite powders were milled by hand using an agate mortar. Figs. 4 and 5 show the SEM and TEM images of the milled composite powders. The composite powders were of nanometer size and slightly aggregated after the simple milling process, irrespective of the post-treatment temperature, as seen in the low-resolution SEM images. The low- and high-resolution TEM images show the detailed microstructures of the composite powders. The powders post-treated at a low temperature of 600 °C consisted of crystals of size several nanometers. The powder shapes were not well defined in the low-resolution TEM images. However, the low- and high-resolution TEM images of the composite powders post-treated at 900 and 1000 °C showed clear polyhedral shapes and well-faceted crystal structures. The mean sizes of the composite powders post-treated at 900 and 1000 °C, measured from the TEM images, were 136 and 265 nm, respectively. The morphologies of the layered $Li(Ni_{1/3}Mn_{1/3}Co_{1/3})O_2$ powders are shown in Fig. 6. The precursor powders prepared under the same conditions as those used in the preparation of the Li_2MnO_3–$Li(Ni_{1/3}Mn_{1/3}Co_{1/3})O_2$ composite powders were post-treated at 900 °C. The layered $Li(Ni_{1/3}Mn_{1/3}Co_{1/3})O_2$ powders had a mean size of 233 nm and highly aggregated structure. When two solid phases are mixed, each phase prevents the crystal growth of the other phase. The composite powders therefore have low mean crystallite sizes and are fine sized, even at a high post-treatment temperature of 1000 °C.

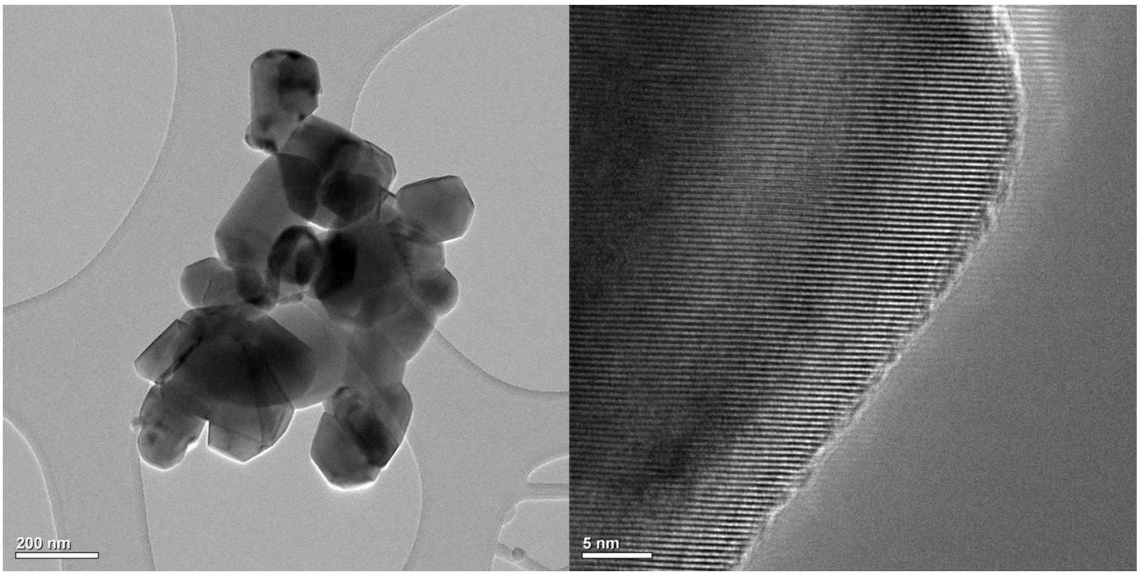

Figure 6. TEM images of the nanosized $Li(Ni_{1/3}Co_{1/3}Mn_{1/3})O_2$ powders post-treated at 900^oC.

The initial charge/discharge curves of the nanosized $0.6Li_2MnO_3$–$0.4Li(Ni_{1/3}Mn_{1/3}Co_{1/3})O_2$ composite cathode powders post-treated at various temperatures at a constant current density of 20 mA

g^{-1} between 2.0 and 4.8 V are shown in Fig. 7. Below 4.5 V, the smoothly sloping voltage profiles in the charge curves are attributed to the removal of Li from the $Li(Ni_{1/3}Mn_{1/3}Co_{1/3})O_2$ component [6,42]. The voltage plateaus above 4.5 V are caused by the removal of Li_2O from the Li_2MnO_3 component [43,44]. In the initial charge curves of the cathode powders post-treated at 600 and 700 °C, the voltage plateaus above 4.5 V are not clearly seen.

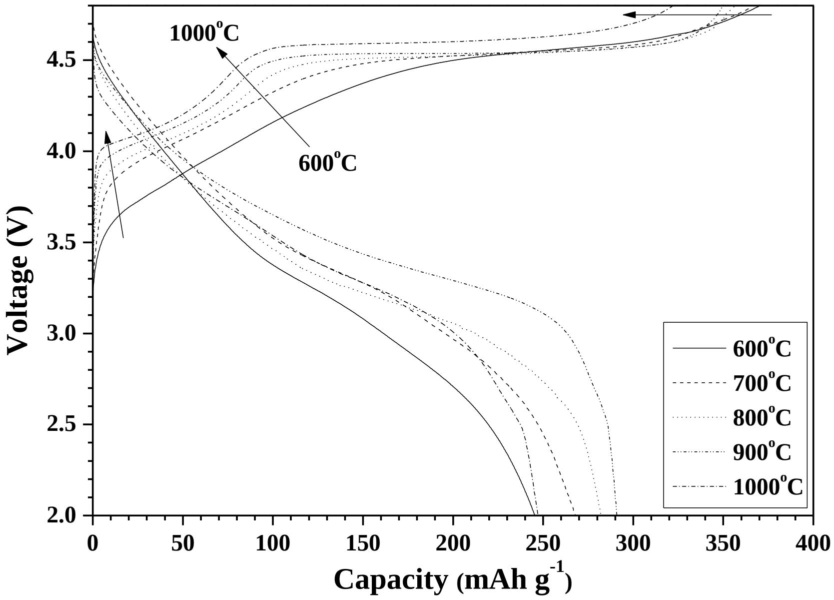

Figure 7. Initial charge/discharge curves of the nanosized composite powders post-treated at various temperatures.

Table 2. Initial charge/discharge capacities and Coulombic efficiencies of the nanosized composite powders post-treated at various temperatures.

	Charge capacity (mAh g^{-1})	Discharge capacity (mAh g^{-1})	Coulombic Efficiency (%)
600 °C	371	245	66
700 °C	367	268	73
800 °C	356	282	79
900 °C	350	291	83
1000 °C	322	247	77

The crystal structures of the Li_2MnO_3 phase were not well observed in the XRD patterns of the powders post-treated at temperatures below 700 °C, as shown in Fig. 2. The composite powders post-treated at 800 and 900 °C had initial charge capacities similar to those of the powders post-treated at 600 and 700 °C. However, the composite powders post-treated at 800 and 900 °C had clear voltage plateaus above 4.5 V. The composite powders post-treated at 1000 °C had low initial charge capacities and low voltage plateaus above 4.5 V. Slight thermal decomposition of the composite powders at 1000 °C decreased the initial charge capacities of the composite powders. The initial charge/discharge capacities and Coulombic efficiencies of the composite powders post-treated at various temperatures are summarized in Table 2. The initial charge capacities decreased from 371 to 350 mAh g^{-1} when the post-treatment temperatures increased from 600 to 900 °C. The initial discharge capacities increased from 245 to 291 mAh g^{-1} for the same temperature changes. The Coulombic efficiencies in the first cycles therefore increased from 66 to 83% when the post-treatment temperatures increased from 600 to 900 °C. The Coulombic efficiency in the first cycle of the composite powders post-treated at 1000 °C was 77%.

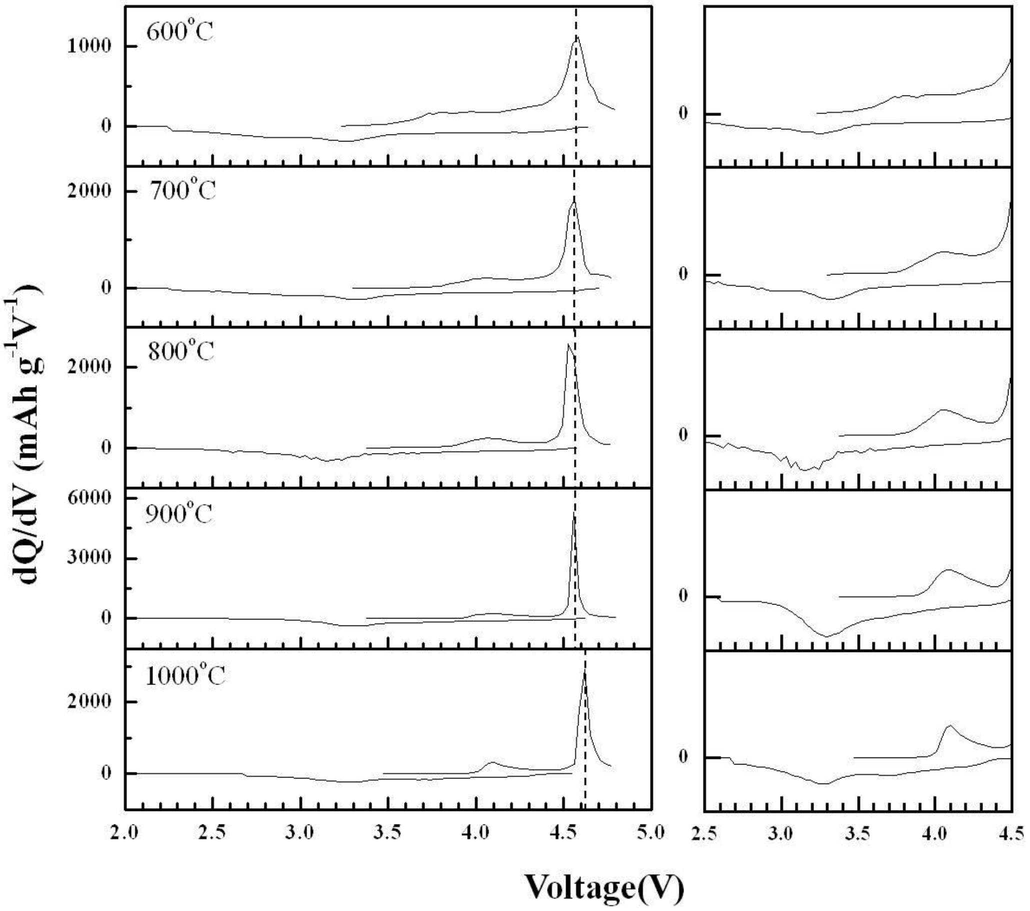

Figure 8. *dQ/dV* curves of the nanosized composite powders post-treated at various temperatures.

Fig. 8 shows the differential capacity vs. voltage (d*Q*/d*V*) curves of the first cycles. The intensities of the oxidation peaks at around 4.6 V resulting from the removal of Li_2O from the Li_2MnO_3 component increased with increasing post-treatment temperature up to 900 °C [5]. This indicates that a large amount of layered Li_2MnO_3 material was formed at a high post-treatment temperature of 900 °C. The oxidation peak at around 4.6 V in the composite powders post-treated at a high temperature of 1000 °C shifted to the high-voltage region. In previous reports, the peaks of composite powders with a large amount of Li_2MnO_3 shifted to the high-voltage region [42]. The removal of Li_2O from the Li_2MnO_3 components of large size or large grain size occurred at high voltages. The composite powders post-treated at 1000 °C had larger mean sizes and mean grain sizes than those of the cathode powders post-treated at temperatures below 900 °C.

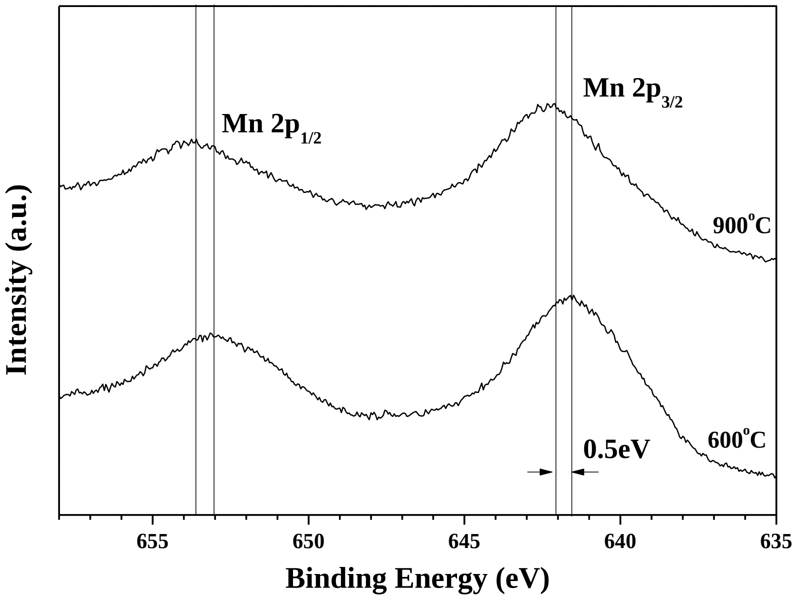

Figure 9. XPS spectra of the Mn 2p in the nanosized composite powders post-treated at 600 and 900 °C.

Fig. 9 shows the Mn 2p XPS spectra of the composite cathode powders post-treated at 600 and 900 °C. The Mn $2p_{3/2}$ binding energies for the cathode powders post-treated at temperatures of 600 and 900 °C were each 641.6 and 642.1 eV. The Mn 2p XPS peaks shifted towards higher binding energies with increasing post-treatment temperatures. The shifts of the Mn 2p XPS peaks towards higher binding energies show an increase in the ratio of Mn^{+4} to Mn^{+3} ions in the cathode powders [44]. The formation of a layered Li_2MnO_3 phase at high post-treatment temperatures of 900 °C shifted the Mn 2p XPS peaks towards higher binding energies.

Fig. 10 shows the Coulombic efficiencies and discharge cycling performances of the composite cathode powders post-treated at various temperatures. The Coulombic efficiencies of the composite powders post-treated at high temperatures of 900 and 1000 °C reached almost 100% from the second cycles. In contrast, the Coulombic efficiencies of the cathode powders post-treated at temperatures below 800 °C reached almost 100% after the fifth or sixth cycles. Lack of the stabilization effect of the Li_2MnO_3 phase and the nanometer sizes below 100 nm of the cathode powders post-treated at temperatures below 800 °C increased the reaction between the cathode powders and the electrolyte. The discharge capacities of the cathode powders post-treated at 600 and 700 °C rapidly decreased within several cycles. The discharge capacities of the cathode powders post-treated at 700 °C decreased from 268 to 188 mAh g^{-1} by the 15th cycle, in which the capacity retention was 70.1%. The cathode powders post-treated at low temperatures, below 700 °C, had poor cycling performances because of the low amount of Li_2MnO_3 phase and low crystallinity. The cycling performances improved with increasing post-treatment temperatures of the cathode powders up to 900 °C. The composite cathode powders with high amounts of the Li_2MnO_3 phase and high crystallinities had good cycling performances. The discharge capacities of the composite cathode powders post-treated at 900 °C decreased from 291 to 269 mA h g^{-1} by the 30th cycle, in which the capacity retention was 92.4%. The cycling performance of the composite cathode powders post-treated at 1000 °C gradually increased up to the fifth cycle.

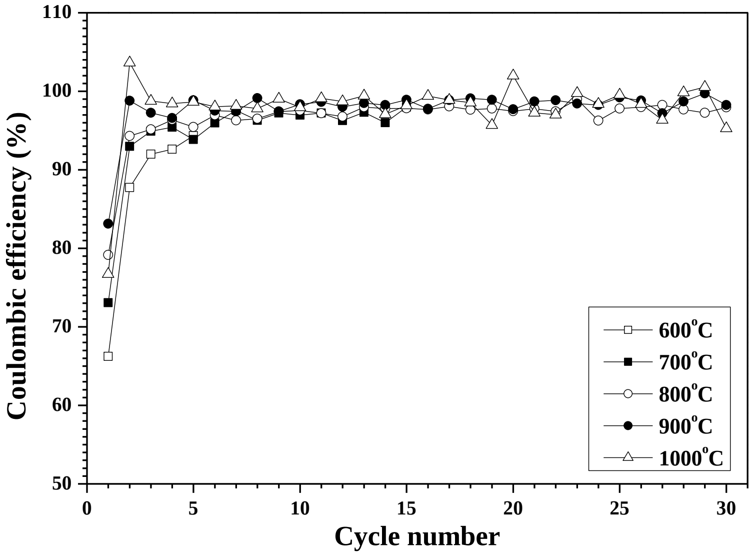

(a) Coulombic efficiency

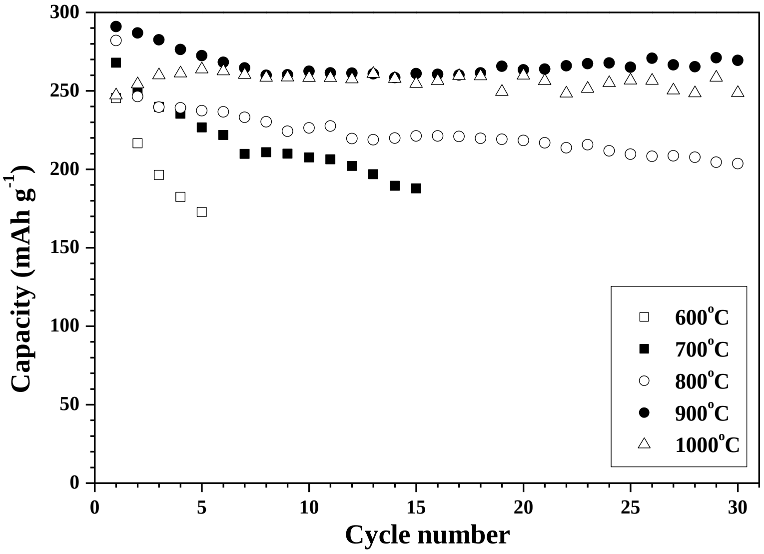

(b) cycling performance

Figure 10. Coulombic efficiencies and cycling performances of the nanosized composite powders post-treated at various temperatures.

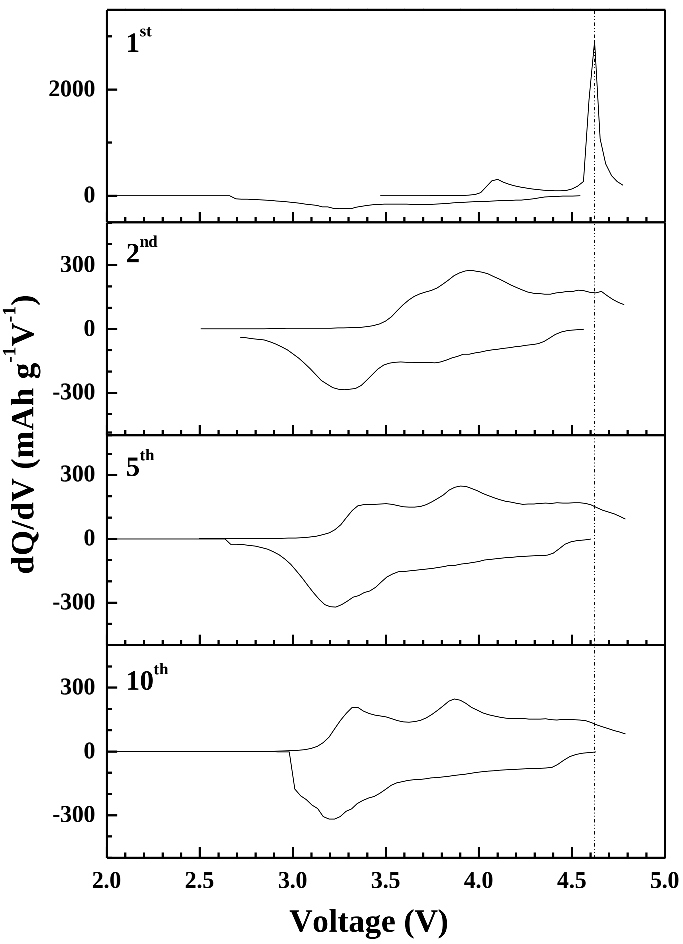

Figure 11. *dQ/dV* curves of the nanosized composite powders post-treated at 1000 °C according to the cycle numbers.

This increase in the capacity with successive cycles can be explained by considering the d*Q*/d*V* curves shown in Fig. 11. The intense oxidation peak at around 4.6 V in the first charge curve disappeared in the subsequent cycles. MnO_2 formed from Li_2MnO_3 by elimination of Li_2O in the initial charge process is gradually transformed into layered $LiMnO_2$ with progressive cycles [45]. The discharge capacities of the post-treated composite powders therefore increase up to the fifth cycle.

4. CONCLUSIONS

The physical and electrochemical properties of $0.6Li_2MnO_3$–$0.4Li(Ni_{1/3}Mn_{1/3}Co_{1/3})O_2$ composite cathode nanopowders prepared by spray pyrolysis from a spray solution with organic additives were investigated. The precursor powders obtained by spray pyrolysis were transformed into nanosized composite powders after post-treatment at temperatures of 600 and 1000 °C, followed by a simple milling process. The layered–layered composite powders were smaller than the layered

$Li(Ni_{1/3}Mn_{1/3}Co_{1/3})O_2$ powders prepared under the same conditions. In the composite cathode powders, each phase prevents the crystal growth of the other phase. The composite powders therefore had low mean crystallite sizes and fine sizes, even at a high post-treatment temperature of 1000 °C. The composite cathode nanopowders with high amounts of the Li_2MnO_3 phase and high crystallinities had high initial charge/discharge capacities and good cycling performances.

ACKNOWLEDGEMENT
This work was supported by the National Research Foundation of Korea(NRF) grant funded by the Korea government(MEST) (No. 2012R1A2A2A02046367).

References

1. S.H. Kang, P. Kempgens, S. Greenbaum, A.J. Kropf, K. Amine, M.M. Thackeray, *J. Mater. Chem.*, 17 (2007) 2069.
2. C.S. Johnson, N. Li, C. Lefief, M.M. Thackeray, *Electrochem. Commun*., 9 (2007) 787.
3. C.S. Johnson, N. Li, C. Lefief, J.T. Vaughey, M.M. Thackeray, *Chem. Mater*., 20 (2008) 6095.
4. M.M. Thackeray, S.H. Kang, C.S. Johnson, J.T. Vaughey, S.A. Hackney, *Electrochem. Commun*., 8 (2006) 1531.
5. C.S. Johnson, J.-S. Kim, C. Lefief, N. Li, J.T. Vaughey, M.M. Thackeray, *Electrochem. Commun*., 6 (2004) 1085.
6. J.M. Zheng, X.B. Wu, Y. Yang, *Electrochim. Acta*, 56 (2011) 3071.
7. Y. Wu, A. Manthiram, *Electrochem. Solid-State Lett*., 9 (2006) A221.
8. J.L. Liu, J. Wang, Y.Y. Xia, *Electrochim. Acta*, 56 (2011) 7392.
9. C. Gan, H. Zhan, X. Hu, Y. Zhou, *Electrochem. Commun*., 7 (2005) 1318.
10. R. Santhanam, B. Rambabu, *Int. J. Electrochem. Sci.*, 4 (2009) 1770.
11. B. Ammundsen, J. Paulsen, *Adv. Mater*., 13 (2001) 943.
12. C.H. Lei, J. Bareno, J.G. Wen, I. Petrov, S.H. Kang, D.P. Abraham, *J. Power Sources*, 178 (2008) 422.
13. A. Ito, D.C. Li, Y. Sato, M. Arao, M. Watanabe, M. Hatano, H. Horie, Y. Ohsawa, *J. Power Sources*, 195 (2010) 567.
14. Z. Li, F. Du, X.F. Bie, D. Zhang, Y.M. Cai, X.R. Cui, C.Z. Wang, G. Chen, Y.J. Wei, *J. Phys. Chem. C*, 114 (2010) 22751.
15. A. van Bommel, J.R. Dahn, *Electrochem. Solid-State Lett.*, 13 (2010) A62.
16. G.S. Nagarajan, J.W. Van Zee, R.W. Spotnitz, *J. Electrochem. Soc*., 145 (1998) 771.
17. J.M. Tarascon, E. Wang, F.K. Shokoohi, W.R. McKinnon, S. Colson, *J. Electrochem. Soc*., 138 (1991) 2859.
18. A. L. Tipton, S. Passerini, B. B. Owens, W. H. Smyrl, *J. Electrochem. Soc*., 143 (1996) 3473.
19. F. Coustier, S. Passerini, W. H. Smyrl, *J. Electrochem. Soc*., 145 (1998) L73.
20. I.A. Courtney, J.R. Dahn, *J. Electrochem. Soc*., 144 (1997) 2943.
21. J.O. Besenhard, J. Yang, M. Winter, *J. Power Sources*, 68 (1997) 87.
22. R. Santhanam, B. Rambabu, *J. Power Sources*, 195 (2010) 4313.
23. Y.J. Wei, K. Nikolowski, S.Y. Zhan, H. Ehrenberg, S. Oswald, G. Chen, C.Z. Wang, H. Chen, *Electrochem. Commun*., 11 (2009) 2008.
24. Y.G. Guo, J.S. Hu, L.J. Wan, *Adv. Mater*., 20 (2008) 2878.
25. Y. Wang, G. Cao, *Adv. Mater*., 20 (2008) 2251.
26. P.G. Bruce, B. Scrosati, J.M. Tarascon, *Angew. Chem. Int. Ed*., 47 (2008) 2930.
27. I. Taniguchi, D. Song, M. Wakihara, *J. Power Sources*, 109 (2002) 333.

28. S.H. Park, Y.K. Sun, *Electrochim. Acta*, 50 (2004) 431.
29. S.W. Oh, S.H. Park, C.W. Park, Y.K. Sun, *Solid State Ionics*, 171 (2004) 167.
30. K. Matsuda, I. Taniguchi, *J. Power Sources*, 132 (2004) 156.
31. K.S. Kim, S.W. Lee, H.S. Moon, H.J. Kim, B.W. Cho, W.I. Cho, J.B. Choi, J.W. Park, *J. Power Sources*, 129 (2004) 319.
32. S.H. Park, Y. Sato, J.K. Kim, Y.S. Lee, *Mater. Chem. Phys*., 102 (2007) 225.
33. C.S. Johnson, N. Li, J.T. Vaughey, S.A. Hackney, M.M. Thackeray, *Electrochem. Commun*., 7 (2005) 528.
34. Z. Lu, J.R. Dahn, *J. Electrochem. Soc*., 149 (2002) A815.
35. S.H. Ju, Y.C. Kang, *Ceram. Int*., 35 (2009) 1633.
36. Y. N. Ko, J. H. Kim, Y. J. Hong, Y. C. Kang, *Mater. Chem. Phys*., 131 (2011) 292.
37. Z. Lu, L.Y. Beaulieu, A. Donaberger, C.L. Thomas, J.R. Dahn, *J. Electrochem. Soc.,* 149 (2002) A778.
38. M.M. Thackeray, S.H. Kang, C.S. Johnson, J.T. Vaughey, R. Benedek, S.A. Hackney, *J. Mater. Chem*., 17 (2007) 3112.
39. Z. Lu, Z. Chen, J.R. Dahn, *Chem. Mater*., 15 (2003) 3214.
40. T.A. Arunkumar, C. Alvarez, A. Manthiram, *J. Electrochem. Soc*., 154 (2007) A770.
41. J. Wang, Y. Xia, X. Yao, M. Zhang, Y. Zhang, Z. Liu, *Int. J. Electrochem. Sci*., 6 (2011) 6670.
42. J.H. Lim, H. Bang, K.S. Lee, K. Amine, Y.K. Sun, *J. Power Sources*, 189 (2009) 571.
43. S.J. Jin, K.S. Park, C.H. Song, M.H. Cho, K.S. Nahm, Y.B. Hahn. Y.S. Lee, *J. Power Sources*, 146 (2005) 630.
44. V.R. Galakhov, M.A. Korotin, N.A. Ovechkina, E.Z. Kurmaev, V.S. Gorshkov, D.G. Kellerman, S. Bartkowski, M. Neumann, *Eur. Phys. J. B*, 14 (2000) 281.
45. S.K. Martha, J. Nanda, G.M. Veith, N.J. Dudney, *J. Power Sources*, 199 (2012) 220.